THE JOURNAL OF PHYSICAL CHEMISTRY C

Article

pubs.acs.org/JPCC

Managing Carrier Lifetime and Doping Property of Lead Halide Perovskite by Postannealing Processes for Highly Efficient Perovskite Solar Cells

Dandan Song,[†] Peng Cui,[†] Tianyue Wang,[†] Dong Wei,[†] Meicheng Li,[*,†,‡] Fanghao Cao,[†,§] Xiaopeng Yue,[†] Pengfei Fu,[†] Yaoyao Li,[†] Yue He,[†] Bing Jiang,[†] and Mwenya Trevor[†]

[†]State Key Laboratory of Alternate Electrical Power System with Renewable Energy Sources, School of Renewable Energy, North China Electric Power University, Beijing 102206, China

[‡]Chongqing Materials Research Institute, Chongqing 400707, China

[§]Department of Chemistry and Pharmacy, Zhuhai College of Jilin University, Zhuhai 519041, China

ABSTRACT: The carrier lifetime and the doping property of the lead halide perovskites are essential factors determining their application in solar cells. Hence, these two factors of the perovskite ($CH_3NH_3PbI_3$) film were managed by postannealing, and the underlying mechanisms governing their effects on the photovoltaic performance of the solar cells were investigated. The short carrier lifetime from electron-hole bimolecular recombination, corresponding to the fast decay of photoluminescence, is achieved in perovskite films annealed at high temperatures. The doping property of the perovskite varies from p-type, intrinsic to n-type with increasing annealing temperature. The short carrier lifetime and the intrinsic feature of the perovskite benefit for high open circuit voltage of the corresponding solar cells, whereas the n-type doped perovskite leads to the high photocurrent and efficiency. Through the management of the carrier lifetime and the doping property, highly efficient perovskite solar cells with conversion efficiency over 17% were prepared. These results provide new insights into the underlying relations between the perovskite properties and the device performance.

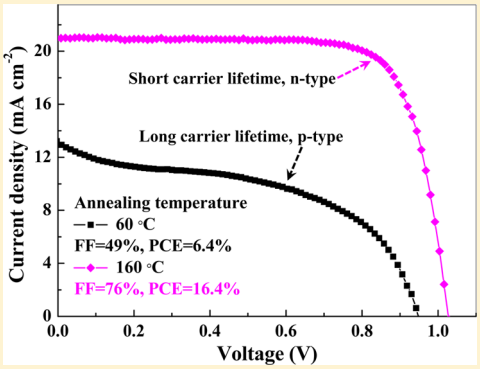

Lead halide perovskite materials ($CH_3NH_3PbX_3$, X = Cl, Br, and I) have shown great promise for application as active materials in solar cells in the past several years.[1−5] The power conversion efficiency (PCE) of lead halide perovskite based thin film photovoltaic devices has increased to more than 20%.[5,6] Carrier lifetime measured by transient photoluminescence (PL) decay is one of the key parameters evaluating the film quality of the perovskites.[7−9] The recombination kinetics of photogenerated carriers have been described as trap-assisted monomolecular recombination or the combination of trap-assisted monomolecular recombination and electron-hole bimolecular recombination.[10] The presence of bimolecular recombination accelerates the PL decay, which shows a much shorter carrier lifetime. Typically, it is considered that longer carrier lifetime indicates better film quality and device performance,[9−12] especially in the condition of the carrier recombination governed by the monomolecular recombination. However, it is also proposed that bimolecular recombination promotes high device performance. Because large perovskite grains with few trap states shows bimolecular recombination and high device efficiency, whereas the perovskite films with trap states presents monomolecular recombination and low device efficiency.[13] Hence, the underlying relations between carrier lifetime and device performance are still open questions and need to be further addressed.

Meanwhile, the perovskite shows high carrier mobility for electrons and/or holes,[14−17] making its performance excellent in perovskite solar cells. The perovskite ($CH_3NH_3PbI_3$) without intentional doping can be p-type[16] or n-type[17] due to the presence of the defects induced by vacancies or interstitials.[18] In most kinds of the solar cells, the doping of active materials is essential for the formation of the p−n junction to separate the carriers and reduce carrier recombination in the heterojunction. Hence, p-type or n-type doping of the perovskite enables it to establish heterojunction with other materials.[19−22] However, the doping of the perovskite is found to deteriorate photovoltaic performance of the solar cells, deriving from the reduced carrier mobility by the large amount of scattering centers in the doped perovskite.[23] Therefore, the correlation between the doping property and the device performance is still unclear.

Here, we managed the carrier lifetime and the doping property of the perovskite ($CH_3NH_3PbI_3$) films and explored the underlying relations between film properties and photovoltaic performance of the solar cells. It is shown that shorter carrier lifetime induced by the bimolecular recombination and

Received: July 16, 2015
Revised: September 16, 2015
Published: September 21, 2015

ACS Publications © 2015 American Chemical Society

DOI: 10.1021/acs.jpcc.5b06859
J. Phys. Chem. C 2015, 119, 22812−22819

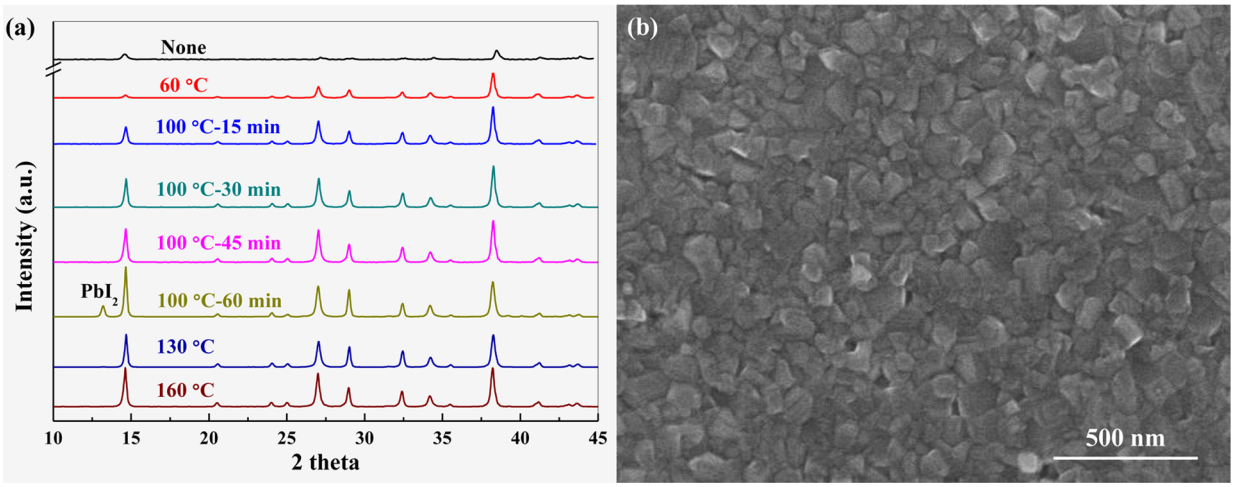

Figure 1. (a) XRD spectra and (b) typical SEM image of the as-fabricated perovskite films.

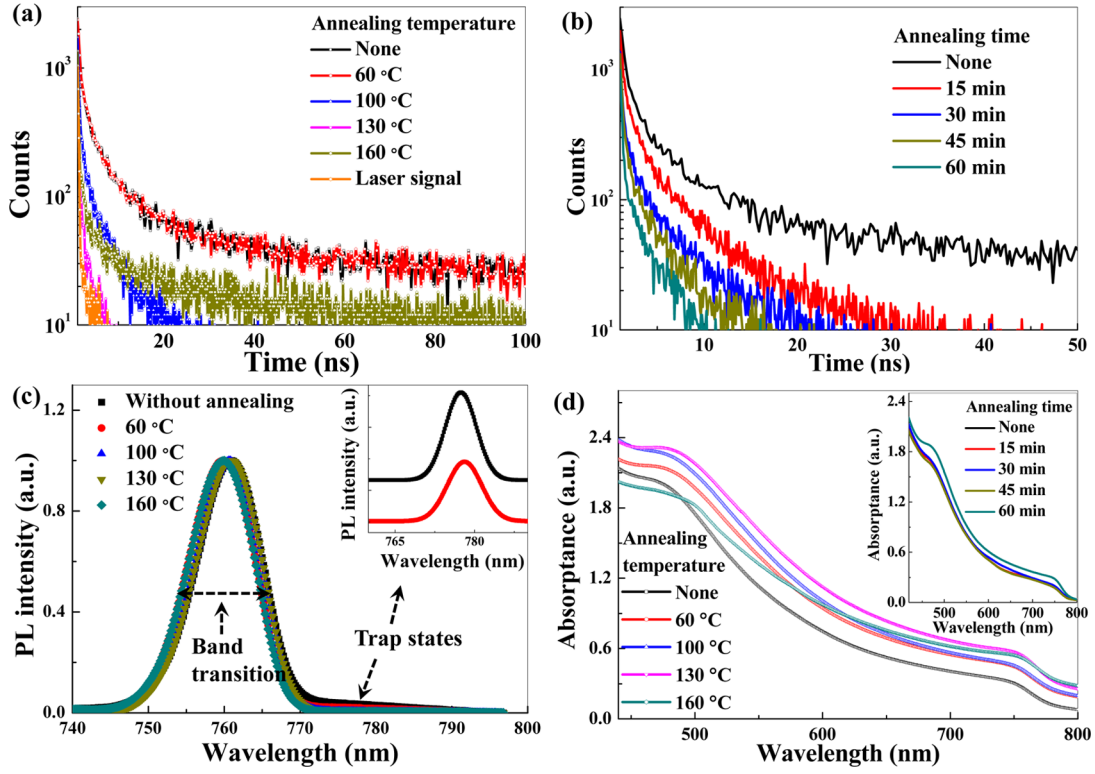

Figure 2. Transient PL decay profiles of the perovskites annealed at (a) different temperatures and for (b) different times excited by a 635 nm pulse laser. (c) Steady PL spectra and (d) absorption spectra of the perovskite films annealed at different parameters. The inset of (c) shows the trap states assisted PL spectra extracted from the whole PL spectra by gaussian fitting.

intrinsic doping of the perovskite favor high open circuit voltage of the related solar cells. The unintentionally n-type doped perovskite leads to higher photocurrent and device efficiency. The solar cells based on perovskite films with short carrier lifetime and the n-doping feature exhibit high power conversion efficiency over 17%.

The as-fabricated perovskite films, with a sequential, solution-processed deposition method from PbI_2 and CH_3NH_3I solutions, all exhibit the typical tetragonal crystalline structure, as evidenced by X-ray diffraction (XRD) and scanning electron microscope (SEM) measurements. As shown by XRD spectra in Figure 1a, all of the perovskite films present the typical tetragonal crystalline structure with diffraction peaks located at 14.6° and 29.0° corresponding to the (110) and (220) planes.[3] The peaks located at 38.2° represent (200) planes of F-doped tin oxide (FTO) substrates. It is also observed that after the postannealing process, the crystallinity of the perovskite film is improved with relatively high diffraction intensities. In the case of annealing at 100 °C for 60 min, a diffraction peak located at 13.2° representing the (001) plane of PbI_2 hexagonal 2H polytype phase[24] is observed, which indicates that the perovskite is decomposed to PbI_2 by some extent after annealing for a long time. The typical SEM image of the perovskite films is shown in Figure 1b. The film shows high quality with multiple grains covering compactly on the substrate. No pinholes are observed in these films.

DOI: 10.1021/acs.jpcc.5b06859
J. Phys. Chem. C 2015, 119, 22812−22819

Table 1. Photoluminescence (PL) Decay Parameters, Emission Peak, and Emission Sites of the Perovskite Films Prepared under Different Post-Annealing Processes

annealing parameters	none	60 °C	100 °C	130 °C	160 °C
bimolecular recombination rate (s^{-1}) at 0–20 ns[a]	4.0×10^8	4.0×10^8	8.2×10^8	8.8×10^8	8.3×10^8
monomolecular recombination lifetime (s) at 20–100 ns	44.0 ± 1.8	44.9 ± 2.0	/	/	27.6 ± 2.0
absorption coefficient (cm^{-1}) at 635 nm	2.9×10^4	3.7×10^4	3.9×10^4	4.5×10^4	4.0×10^4
emission peak (nm)	760, 778	760, 778	760	760	760
emission sites	less	less	more	more	more

[a]The recombination rate constant a equals $B\Delta n_0$, where B and Δn_0 represent bimolecular recombination coefficient ($cm^3\ s^{-1}$) and the excess carrier concentration (cm^{-3}) at $t = 0$.

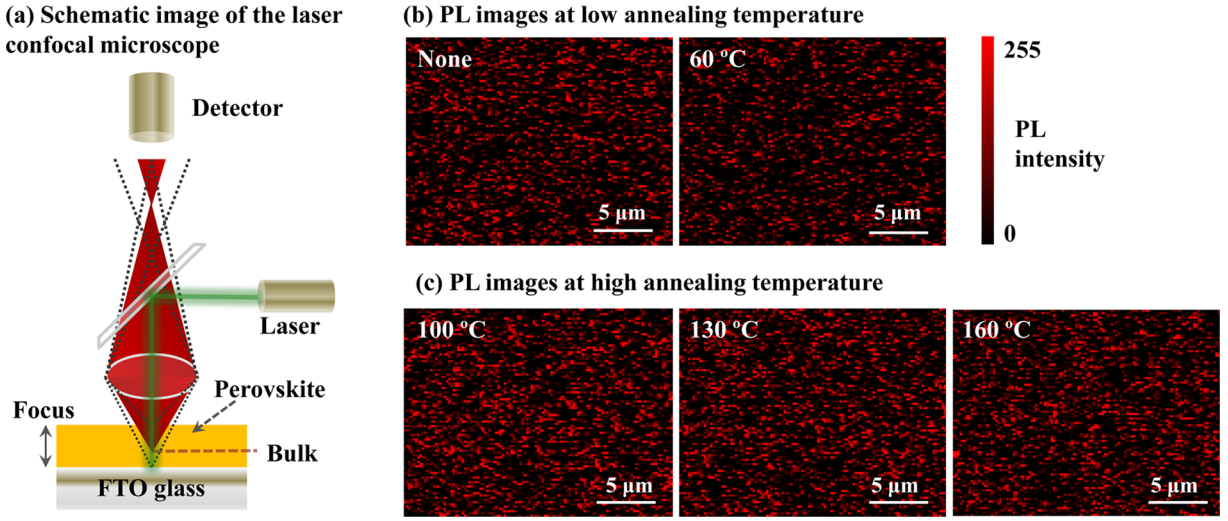

Figure 3. (a) Schematic image of the laser confocal microscopy and (b and c) the measured spatial PL images from the perovskite films annealed at low and high temperatures, respectively.

The Transient photoluminescence (PL) technique is employed to estimate carrier lifetime, and the decay curves measured from the perovskite films on glass substrates annealed at different temperatures are shown in Figure 2a. In general, the PL decay profile depends heavily on both of the film performance and the excitation energy.[10,25] Here, the excitation energy of the perovskite films is nearly identical, which is lower than 3 nJ/cm^2 and causes the PL decay curves to present stretching exponential profiles. As shown in Figure 2a, PL decay is governed by a fast bimolecular recombination process (short carrier lifetime) at the initial stage and slow monomolecular recombination (long carrier lifetime) at the long time scale. In perovskites, bimolecular recombination is caused by the recombination of photogenerated electrons and holes, whereas monomolecular recombination is from photoexcited carriers and unintentionally doped carriers (trap states).[10] From the decay profiles of the perovskite films, it is clear that the proportion of monomolecular recombination first decreases with increasing annealing temperature and then increases in the condition of 160 °C. In addition, the proportion of monomolecular recombination also decreases with increasing annealing time, as shown in Figure 2b. The bimolecular recombination rate a and the monomolecular recombination lifetime τ were estimated by fitting the decay curves with the expressions $I = I_0(1 + at)^{-2}$ and $I = I_0e^{-t/\tau}$, respectively. The results are listed in Table 1.

From Table 1, it is clear that bimolecular recombination rate is high in perovskite films annealed at high temperature, whereas monomolecular recombination is more obvious in perovskite films annealed at lower temperature and 160 °C. The dominant bimolecular recombination is found to be accompanied by less trap states and benefit for highly efficient solar cells.[13] In this context, the bimolecular recombination in perovskite films annealed at high temperature is also probably correlated with the reduced trap states. The radiative trap states are investigated by steady PL spectra, as shown in Figure 2c. For the condition of perovskite annealed at low temperature, a PL peak located at 778 nm can be observed, which represents trap-assisted emission.[26] Upon increasing the annealing temperature, only the emission peaked at 760 nm from the interband transition between the electrons in the conduction band and the holes in the valence band are observed, indicating low density of radiative trap states in these perovskite films. Hence, trap-assisted monomolecular recombination is weak in these films. It is worth noting that the changes in PL decay and spectra with annealing temperature are not caused by the change in excitation intensity. The excitation energy is set to be identical for all of the films, whereas the absorption intensities of these films are also similar. As shown in Figure 2d and Table 1, the variation of the absorption intensity varies with annealing temperature and time is not consistent with that of the PL decay, implying the differences in absorption intensities are not the origins for the variation of the PL decay.

The varied nonradiative trap states in the perovskite films by the annealing temperature are also characterized using a confocal laser microscope, which measures the spatial distribution of the emission sites in the films. Schematic illustration of the confocal laser microscope is shown in Figure 3a. The focus can be adjusted, which enables the characterization of the emission from different regions. Here, to avoid

DOI: 10.1021/acs.jpcc.5b06859
J. Phys. Chem. C 2015, 119, 22812–22819

the surface effect, PL images were recorded in the condition of the focus locating in the bulk. The spatial PL images from the perovskites annealed at different temperatures are shown in Figure 3 (panels b and c), representing for the cases of low and high annealing temperature, respectively. The emission sites are increased obviously by increasing annealing temperature, which indicates that a lower density of the nonradiative trap states exist in perovskite films annealed at high temperature than that at low temperature.

Hence, the varied PL decay of perovskite films by annealing temperature derives from the modification of the trap states. The reduction of radiative and nonradiative trap states in perovskite film annealed at high temperature is probably associated with less unintentionally doped carriers in the corresponding film. Meanwhile, from the above results and discussion, it can also be seen that long carrier lifetime is not an essential indicator of good film quality of the perovskites. The correlation between carrier lifetime and film quality depends on the origin of recombination processes. Furthermore, it needs to be pointed out that the carriers detected by PL measurements possess a small part of photogenerated carriers. The electron-to-photon conversion ratio of the perovskite (<5%, light-emitting diodes) is much lower than the photon-to-electron conversion ratio (>60%, solar cells),[27] suggesting that lots of carriers contributing to the photocurrent are not radiative and not able to be detected by PL measurements.

To investigate the doping property of the perovskite films, X-ray photoelectron spectroscopy (XPS) measurements were carried out on the perovskite films fabricated on FTO/glass substrates. As shown in Figure 4a, the distance between valence

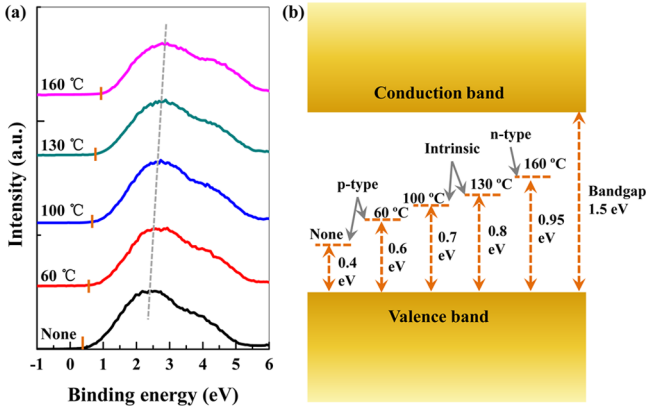

Figure 4. (a) XPS and (b) schematic energy level diagram of the perovskites annealed at different temperatures.

band and Fermi level of the perovskite increases with increasing annealing temperature. The estimated values of the Fermi level refering to the valence band are shown in Figure 4b. The Fermi level locates 0.4 eV away from the valence band in perovskite without annealing, which shifts to 0.95 eV in perovskite annealed at 160 °C. With consideration of its bandgap of 1.5 eV,[28] it is seen that the perovskite presents p-type doping, intrinsic to n-type doping with increasing annealing temperature, as depicted in Figure 4b.

The doping feature of the perovskite films in real devices was also characterized by Mott–Schottky analysis. The Mott–Schottky plot of inverse square capacitance (C^{2-}) versus applied voltage (V) yields a straight line with its slope inversely proportional to the doping concentration, as marked in Figure 5 by the dashed lines. The doping concentration is determined by

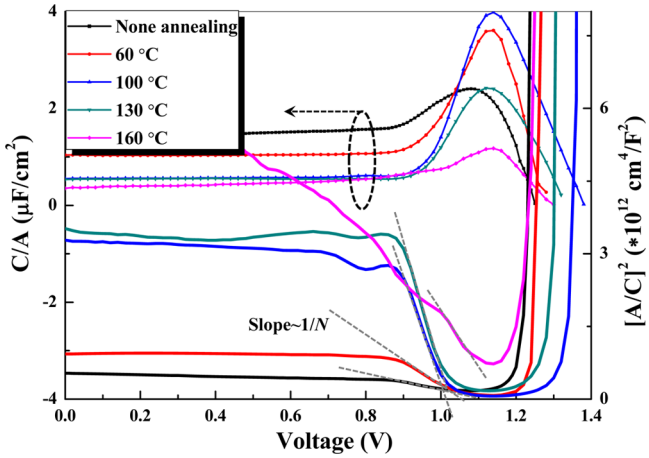

Figure 5. Capacitance–voltage curves and Mott–Schottky plots of the solar cells based on perovskite films annealed at different temperatures.

$$N = -\frac{2}{q\varepsilon}\left(\frac{\mathrm{d}(C/A)^{-2}}{\mathrm{d}V}\right)^{-1}$$

where q, ε, and A represent for electron charge, dielectric constant, and device area, respectively. The calculated N values in condition of $\varepsilon = 200\varepsilon_0$ for perovskite[29] are shown in Table 2, which are comparable to previous reported values for perovskites measured with the Hall Effect measurement.[23] From Figure 5 and Table 2, it can be seen that the doping concentration, which changes inversely with the slope of the Mott–Schottky plot, first increases with increasing annealing temperature and then decreases. Therefore, the doping concentrations in the solar cells with perovskite films annealed at 100 and 130 °C are lower than these in solar cells annealed at other temperatures. As only annealing temperature of the perovskite is varied, the change in the doping concentration of the solar cells reflects the corresponding change in the doping concentration of the perovskite films. Hence, Mott–Schottky analysis reveals the correlation between the doping property and the annealing temperature of perovskite film, which is similar to XPS results.

The high doping concentration leads to enhanced recombination between doped carriers and photocarriers, causing a large proportion of monomolecular recombination in PL decay of the related perovskite films. The doping feature of as-prepared perovskite films derives from the defects. In $CH_3NH_3PbI_3$, the defects with low formation energies are mainly Pb vacancies, I interstitials, and CH_3NH_3 interstitials as calculated by density functional theory (DFT),[18] in which Pb vacancies and I interstitials create p-type doping while CH_3NH_3 interstitials create n-type doping. The as-prepared perovskite crystal without annealing is nonstoichiometric with Pb vacancies and/or I interstitials because the fabrication of perovskite film employs a sequential deposition method in which CH_3NH_3I is excess (the atom ratio of I to Pb exceeds 3 calculated from XPS spectra). With increasing annealing temperature, Pb vacancies and/or I interstitials are reduced, accompanying with the removing of excess CH_3NH_3I, leading to the weakened p-type doping of the films. At even higher temperature (160 °C), the continued removal of CH_3NH_3I

DOI: 10.1021/acs.jpcc.5b06859
J. Phys. Chem. C 2015, 119, 22812–22819

Table 2. Doping Properties of the Perovskite Films Obtained from XPS Measurement and Mott-Schottky Analysis Carried on Perovskite Films and Solar Cells, Respectively

annealing parameters	none	60 °C	100 °C	130 °C	160 °C
doping type	p	p	intrinsic	intrinsic	n
doping concentration (cm^{-3})	5.0×10^{17}	1.5×10^{17}	3.4×10^{16}	2.8×10^{16}	6.3×10^{16}

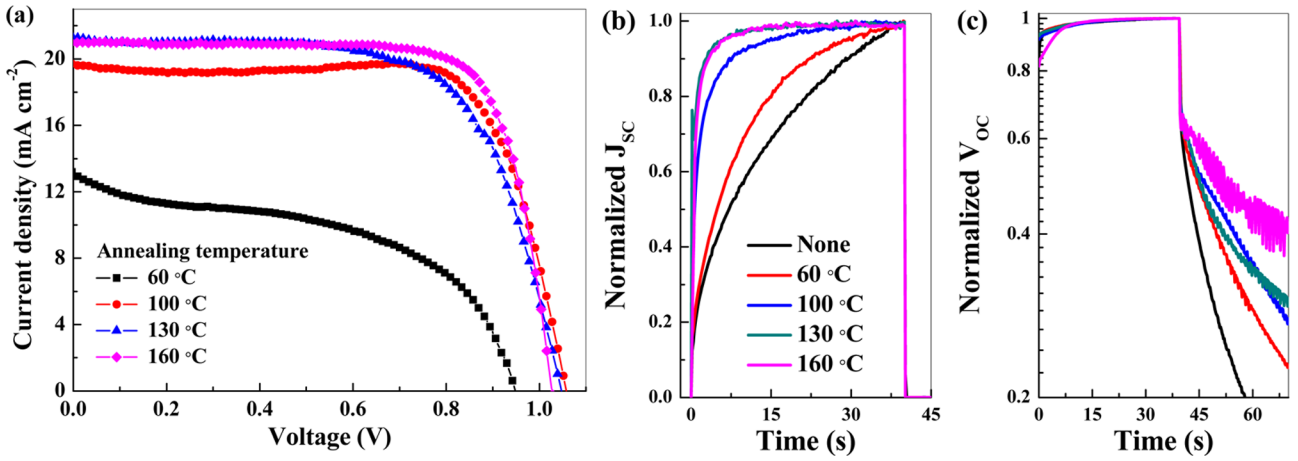

Figure 6. (a) $J-V$ curves of the solar cells with perovskite films annealed at different temperatures. (b) J_{SC} and (c) V_{OC} decay curves of the solar cells. $J-V$ curves were measured in reverse scan.

Table 3. Photovoltaic Parameters of the Solar Cells with Perovskite Films Processed under Different Temperatures[a]

	best values[b]				average values[c]		
annealing temperature	J_{SC} (mA/cm^2)	V_{OC} (V)	FF	PCE (%)	J_{SC} (mA/cm^2)	V_{OC} (V)	PCE (%)
60 °C	12.9	0.95	0.49	6.0	10.8 ± 1.6	0.95 ± 0.03	5.0 ± 1.3
100 °C	19.6	1.06	0.74	15.4	17.9 ± 1.0	1.05 ± 0.01	14.5 ± 1.0
130 °C	21.5	1.01	0.74	16.0	20.6 ± 0.8	1.03 ± 0.02	14.9 ± 0.9
160 °C	21.0	1.02	0.76	16.4	20.8 ± 0.6	1.02 ± 0.01	16.0 ± 0.7

[a]All of the solar cells were fabricated in a same batch. [b]The best values obtained from the solar cells with the highest efficiency. [c]The values and the corresponding standard deviations were obtained by the average of 4 identical cells.

leads to Pb-rich/I-poor condition, and changes the doping property of the perovskite film to be n-type.

The doping property of the perovskite film will influence the photovoltaic performance of the solar cells in two aspects. The first one is its effect on bulk carrier recombination (i.e., doped carriers will increase carrier recombination in perovskite film). The other one is its effect on built-in potential of the solar cells, which will affect carrier distribution and surface/interface recombination. The variations in the carrier distribution and recombination will change short circuit current density (J_{SC}) and/or open circuit voltage (V_{OC}) of the solar cells, leading to the different power conversion efficiencies (PCE).

Photocurrent–voltage ($J-V$) curves of the solar cells using perovskite films with different carrier lifetimes and doping properties are shown in Figure 6a. The photovoltaic parameters including J_{SC}, V_{OC}, fill factor (FF), and PCE are extracted and listed in Table 3. Solar cells with perovskite films annealed at low temperature (60 °C) show lower J_{SC}, V_{OC}, and PCE. With increasing annealing temperature, J_{SC} increases consistently, whereas V_{OC} achieves the highest value in the condition of 100 °C. PCE increases consistently with increasing annealing temperature, reaching an average value of 16.0% at the annealing temperature of 160 °C. It is worth noting that solar cells utilizing perovskite films annealed at 160 °C achieve better performance than these annealed at 100 °C (i.e., the typically used temperature in fabricating perovskite solar cells). By comparing the relations between PL decay and photovoltaic parameters, it can be found that perovskite films with fast PL decay annealed at high temperatures (low carrier lifetime) promote relatively high J_{SC} and PCE. Furthermore, the doping property of the perovskite film plays an important role in determining photovoltaic parameters of the solar cells. The perovskite film without unintentional doping (intrinsic, annealed at 100 and 130 °C) enables high V_{OC} of the related solar cells. The perovskite film with n-type unintentional doping (annealed at 160 °C) enables moderate V_{OC} and high J_{SC}, leading to the highest PCE among the solar cells annealed at different temperatures.

To get an insight in the effect of trap states on photovoltaic performance of the solar cells, transient J_{SC} and V_{OC} profiles were measured. The carriers trapped by the trap states will lead to slow response of the photocurrent through the delay in charge transport by trapping and detrapping processes. The untrapped carriers, either radiative or nonradiative, lead to fast generation of the photocurrent favored by the high mobility of perovskite. As shown in Figure 6b, J_{SC} rises fast in solar cells with perovskite films annealed at high temperature, indicating a large proportion of untrapped carriers in corresponding perovskite films. This observation is in accordance with the deduction from PL measurements. In addition, V_{OC} also shows slow decay in perovskite solar cells annealed at high temperature (Figure 6c), as is consistent with the reduced

DOI: 10.1021/acs.jpcc.5b06859
J. Phys. Chem. C 2015, 119, 22812–22819

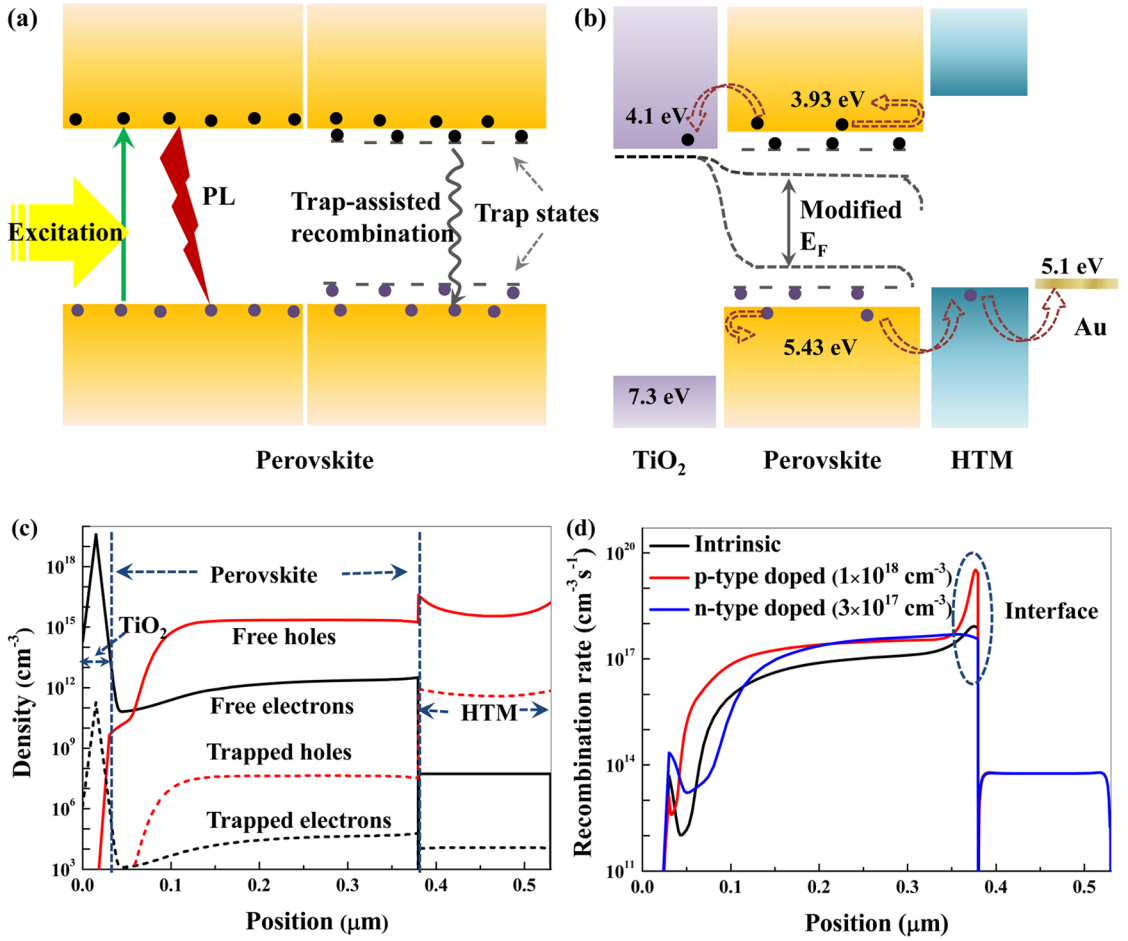

Figure 7. Schematic diagrams of carrier recombination (a) in the perovskite films and (b) working mechanism of the perovskite solar cells. (c) Simulated carrier distribution and (d) recombination in perovskite solar cells.

number of trap states which cause the carrier recombination and reduce the photovoltage.

The underlying mechanism determining the dependencies of device performance on carrier lifetime and doping property of the perovskite films are depicted in Figure 7 (panels a and b). As shown in Figure 7a, in the absence of trap states, the photoexcitation of the perovskite causes the generation of excited electrons and holes, leading to the radiative recombination creating interband luminescence or the long-lived nonradiative carriers. Hence, the detected PL decay is governed by electron-hole bimolecular recombination. In the presence of trap states, as also shown in Figure 7a, numerous excited holes or electrons are trapped, followed by radiative recombination creating trap-assisted luminescence or non-radiative recombination. Therefore, monomolecular recombination induced by the trap-assisted recombination is obvious in perovskite films with more trap states. In perovskite solar cells, as depicted in Figure 7b, the presence of trap states will cause losses in carrier collection, leading to low J_{SC}. Thereby, the solar cells employing perovskite films with slow PL decay (long carrier lifetime), corresponding to the presence of trap states, yield lower J_{SC} than that with fast PL decay (short carrier lifetime).

Meanwhile, the doping property of the perovskite film also affects the device operation. As shown in Figure 7b, perovskite solar cells are based on p-i-n heterojunction established across the TiO_2 /perovskite/hole transport material (HTM) stack. In condition of the doped perovskite, the bulk recombination of minority carriers in the heterojunction is enhanced, leading to reduced V_{OC} in doped solar cells compared to intrinsic solar cells. Meanwhile, the doping property also influences J_{SC} of the solar cells, which is revealed by device simulation with wxAMPS.[30] As shown in Figure 7c, electrons are facilely extracted by TiO_2 from perovskite, whereas holes are accumulated in perovskite and near perovskite/HTM interface in the solar cells with intrinsic perovskite film, deriving from n-type doped character of TiO_2 and the organic feature of HTM. Hence, carrier recombination is obvious in the region approximating the perovskite/HTM interface (Figure 7d). For the condition of p-type doped perovskite (Figure 7d), carrier recombination is more intense near this interface and in the perovskite film, causing significant carrier losses. For the condition of n-type doped perovskite, carrier recombination close to this interface is reduced, due to the enhanced electric field at the perovskite/HTM interface that favors the separation of electrons and holes. The low recombination rate near the perovskite/HTM interface benefits carrier collection, which leads to increased J_{SC} in intrinsic and n-type doped perovskite solar cells.

On the basis of the above mechanisms, it can be deduced that perovskite solar cells with short carrier lifetime and weak n-type doping will exhibit excellent performance. Hence, the solar cells with perovskite films annealed at 150 °C for 30 min, which are supposed to possess shorter carrier lifetime and weaker n-

DOI: 10.1021/acs.jpcc.5b06859
J. Phys. Chem. C 2015, 119, 22812−22819

type doping compared to the perovskite films annealed at 160 °C for 30 min, were prepared. The $J-V$ curve from the device with the best performance is shown in Figure 8. The solar cell

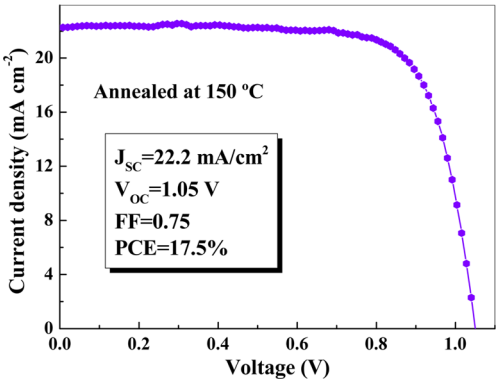

Figure 8. $J-V$ curve of the champion solar cell with perovskite film annealed at 150 °C for 30 min.

yields a J_{SC} of 22.2 mA/cm^2, a V_{OC} of 1.05 V, and a FF of 0.75, leading to a PCE of 17.5%. The average values of the photovoltaic parameters are also estimated from 10 identical solar cells, which show an average J_{SC} of 21.6 mA/cm^2, V_{OC} of 1.03 V, and PCE of 16.5%. All of these parameters are much superior to these from solar cells employing perovskite films annealed at typically used conditions (100 °C), further demonstrating the rationality of designing solar cells by managing carrier lifetime and doping property of the perovskite films.

In conclusion, the management of carrier lifetime and doping property of solution processed, sequential deposited lead halide perovskite films are achieved by postannealing processes and the underlying mechanisms of their effects on device performance are explored. On the basis of the explorations, a rational design of highly efficient perovskite solar cells is proposed (i.e., the perovskite films with short carrier lifetime induced by bimolecular recombination and the weak n-type doping are more efficient in the solar cells). The solar cells employing such kind of perovskite films exhibit high conversion efficiencies with the highest value of 17.5% and the average value of 16.5%. The results provide insights into the inner properties of perovskite films and the related device performance, which also provide an efficient approach for the fabrication of highly efficient perovskite solar cells.

EXPERIMENTAL METHODS

Fabrication of $CH_3NH_3PbI_3$ Films and Solar Cells. $CH_3NH_3PbI_3$ films were fabricated using a sequential deposition process.[2,24] PbI_2 was first loaded by spin-coating from dimethyl sulfoxide onto a compact TiO_2 layer (spin-coated twice for solar cell use) or glass substrates (for photoluminescence measurements) and then dipped into a solution of CH_3NH_3I in ultradry isopropanol for 10 min, leading to the formation of $CH_3NH_3PbI_3$ films followed by postannealing at different temperature and time. All of the procedures were carried out in a glovebox filled with high purity N_2. The solar cells employ the planar architecture of a FTO/compact TiO_2/perovskite (~300 nm)/HTM/Au electrode. A compact TiO_2 layer with a thickness of ~25 nm was fabricated on FTO by $TiCl_4$ treatment.[31] An HTM layer (150 nm) was obtained by spin-coating 2,2′,7,7′-tetrakis[*N*,*N*-di(4-methoxyphenyl)amino]-9,9′-spirobifluorene (spiro-MeOTAD) solution (dissolved in chlorobenzene) with standard additives including *tert*-butylpyridine and lithium bis-(trifluoromethanesulfonyl)imide in the glovebox, followed by oxidation in clean air for 24 h. After that, Au electrode was prepared by magnetron sputtering.

Characterization and Device Simulation. Transient PL decay of the perovskite films on glass substrates was measured using a transient state spectrophotometer (Edinburgh Ins. FL920) under the irradiation of a 635 nm pulse laser with excitation energy around 3 nJ/cm^2. Laser confocal microscope measurement of the perovskite films on glass substrates were conducted using Leica TCS-SP5 with a 532 nm laser. Capacitance−voltage and Mott−Schottky plots of the solar cells with perovskite films annealed at different temperatures were measured by an electrochemical working station (Zahner Zennium) with a frequency of 500 Hz. Current−voltage curves were measured using a source meter (Keithley 2400) under AM 1.5G irradiation with a power density of 100 mW/cm^2 from a solar simulator (XES-301S+EL-100). Device simulation was carried out using wxAMPS software, based on the planar architecture of a FTO/compact TiO_2 (30 nm)/perovskite (350 nm)/ HTM (150 nm)/Au electrode. The doping concentrations, mobility, and other properties of the materials were reference in the literature.[15,23,32−34]

AUTHOR INFORMATION

Corresponding Author

*E-mail: mcli@ncepu.edu.cn. Tel: +86 10 6177 2951. Fax: +86 10 6177 2951.

Notes

The authors declare no competing financial interest.

ACKNOWLEDGMENTS

This work was supported partially by National High-tech R&D Program of China (863 Program, Grant 2015AA034601), National Natural Science Foundation of China (Grants 91333122, 51402106, 51372082, 51172069, 61204064, and 51202067), Ph.D. Programs Foundation of Ministry of Education of China (Grants 20120036120006 and 20130036110012), Par-Eu Scholars Program, and the Fundamental Research Funds for the Central Universities.

REFERENCES

(1) Lee, M. M.; Teuscher, J.; Miyasaka, T.; Murakami, T. N.; Snaith, H. J. Efficient Hybrid Solar Cells based on Meso-Superstructured Organometal Halide Perovskites. *Science* **2012**, *338*, 643−647.

(2) Burschka, J.; Pellet, N.; Moon, S.-J.; Humphry-Baker, R.; Gao, P.; Nazeeruddin, M. K.; Grätzel, M. Sequential Deposition as a Route to High-Performance Perovskite-Sensitized Solar Cells. *Nature* **2013**, *499*, 316−319.

(3) Kojima, A.; Teshima, K.; Shirai, Y.; Miyasaka, T. Organometal Halide Perovskites as Visible-Light Sensitizers for Photovoltaic Cells. *J. Am. Chem. Soc.* **2009**, *131*, 6050−6051.

(4) Kim, H.-S.; Lee, C.-R.; Im, J.-H.; Lee, K.-B.; Moehl, T.; Marchioro, A.; Moon, S.-J.; Humphry-Baker, R.; Yum, J.-H.; Moser, J. E.; Gratzel, M.; Park, N.-G. Lead Iodide Perovskite Sensitized All-Solid-State Submicron Thin Film Mesoscopic Solar Cell with Efficiency Exceeding 9%. *Sci. Rep.* **2012**, *2*, 591.

(5) Im, J.-H.; Lee, C.-R.; Lee, J.-W.; Park, S.-W.; Park, N.-G. 6.5% Efficient Perovskite Quantum-Dot-Sensitized Solar Cell. *Nanoscale* **2011**, *3*, 4088−4093.

(6) Yang, W. S.; Noh, J. H.; Jeon, N. J.; Kim, Y. C.; Ryu, S.; Seo, J.; Seok, S. I. High-Performance Photovoltaic Perovskite Layers

DOI: 10.1021/acs.jpcc.5b06859
J. Phys. Chem. C 2015, 119, 22812−22819

Fabricated through Intramolecular Exchange. *Science* **2015**, *348*, 1234−1237.
(7) Stranks, S. D.; Eperon, G. E.; Grancini, G.; Menelaou, C.; Alcocer, M. J.; Leijtens, T.; Herz, L. M.; Petrozza, A.; Snaith, H. J. Electron-hole diffusion lengths exceeding 1 micrometer in an Organometal Trihalide Perovskite Absorber. *Science* **2013**, *342*, 341−344.
(8) Xing, G.; Mathews, N.; Sun, S.; Lim, S. S.; Lam, Y. M.; Grätzel, M.; Mhaisalkar, S.; Sum, T. C. Long-Range Balanced Electron- and Hole-Transport Lengths in Organic-Inorganic $CH_3NH_3PbI_3$. *Science* **2013**, *342*, 344−347.
(9) de Quilettes, D. W.; Stranks, S. D.; Nagaoka, H.; Eperon, G. E.; Ziffer, M. E.; Snaith, H. J.; Ginger, D. S.; Vorpahl, S. M. Impact of Microstructure on Local Carrier Lifetime in Perovskite Solar Cells. *Science* **2015**, *348*, 683−686.
(10) Yamada, Y.; Nakamura, T.; Endo, M.; Wakamiya, A.; Kanemitsu, Y. Photocarrier Recombination Dynamics in Perovskite $CH_3NH_3PbI_3$ for Solar Cell Applications. *J. Am. Chem. Soc.* **2014**, *136*, 11610−11613.
(11) Zhou, H.; Chen, Q.; Li, G.; Luo, S.; Song, T.-b.; Duan, H.-S.; Hong, Z.; You, J.; Liu, Y.; Yang, Y. Interface Engineering of Highly Efficient Perovskite Solar Cells. *Science* **2014**, *345*, 542−546.
(12) Liang, P. W.; Liao, C. Y.; Chueh, C. C.; Zuo, F.; Williams, S. T.; Xin, X. K.; Lin, J.; Jen, A. K. Y. Additive Enhanced Crystallization of Solution-Processed Perovskite for Highly Efficient Planar-Heterojunction Solar Cells. *Adv. Mater.* **2014**, *26*, 3748−3754.
(13) Nie, W.; Tsai, H.; Asadpour, R.; Blancon, J.-C.; Neukirch, A. J.; Gupta, G.; Crochet, J. J.; Chhowalla, M.; Tretiak, S.; Alam, M. A.; Wang, H.-L.; Mohite, A. D. High-Efficiency Solution-Processed Perovskite Solar Cells with Millimeter-Scale Grains. *Science* **2015**, *347*, 522−525.
(14) Grätzel, M. The Light and Shade of Perovskite Solar Cells. *Nat. Mater.* **2014**, *13*, 838−842.
(15) Wehrenfennig, C.; Eperon, G. E.; Johnston, M. B.; Snaith, H. J.; Herz, L. M. High Charge Carrier Mobilities and Lifetimes in Organolead Trihalide Perovskites. *Adv. Mater.* **2014**, *26*, 1584−1589.
(16) Bi, C.; Shao, Y.; Yuan, Y.; Xiao, Z.; Wang, C.; Gao, Y.; Huang, J. Understanding the Formation and Evolution of Interdiffusion Grown Organolead Halide Perovskite Thin Films by Thermal Annealing. *J. Mater. Chem. A* **2014**, *2*, 18508−18514.
(17) Stoumpos, C. C.; Malliakas, C. D.; Kanatzidis, M. G. Semiconducting tin and Lead Iodide Perovskites with Organic Cations: Phase Transitions, High Mobilities, and Near-infrared Photoluminescent Properties. *Inorg. Chem.* **2013**, *52*, 9019−9038.
(18) Yin, W.-J.; Shi, T.; Yan, Y. Unusual Defect Physics in $CH_3NH_3PbI_3$ Perovskite Solar Cell Absorber. *Appl. Phys. Lett.* **2014**, *104*, 063903.
(19) Mei, A.; Li, X.; Liu, L.; Ku, Z.; Liu, T.; Rong, Y.; Xu, M.; Hu, M.; Chen, J.; Yang, Y.; Gratzel, M.; Han, H. A Hole-Conductor-Free, Fully Printable Mesoscopic Perovskite Solar Cell with High Stability. *Science* **2014**, *345*, 295−298.
(20) Etgar, L.; Gao, P.; Xue, Z.; Peng, Q.; Chandiran, A. K.; Liu, B.; Nazeeruddin, M. K.; Grätzel, M. Mesoscopic $CH_3NH_3PbI_3/TiO_2$ Heterojunction Solar Cells. *J. Am. Chem. Soc.* **2012**, *134*, 17396−17399.
(21) Laban, W. A.; Etgar, L. Depleted Hole Conductor-Free Lead Halide Iodide Heterojunction Solar Cells. *Energy Environ. Sci.* **2013**, *6*, 3249−3253.
(22) Liu, D.; Yang, J.; Kelly, T. L. Compact Layer Free Perovskite Solar Cells with 13.5% Efficiency. *J. Am. Chem. Soc.* **2014**, *136*, 17116−17122.
(23) Wang, Q.; Shao, Y.; Xie, H.; Lyu, L.; Liu, X.; Gao, Y.; Huang, J. Qualifying Composition Dependent p and n Self-Doping in $CH_3NH_3PbI_3$. *Appl. Phys. Lett.* **2014**, *105*, 163508.
(24) Wu, Y.; Islam, A.; Yang, X.; Qin, C.; Liu, J.; Zhang, K.; Peng, W.; Han, L. Retarding the Crystallization of PbI_2 for Highly Reproducible Planar-Structured Perovskite Solar Cells via Sequential Deposition. *Energy Environ. Sci.* **2014**, *7*, 2934−2938.
(25) Yamada, Y.; Endo, M.; Wakamiya, A.; Kanemitsu, Y. Spontaneous Defect Annihilation in $CH_3NH_3PbI_3$ Thin Films at Room Temperature Revealed by Time-Resolved Photoluminescence Spectroscopy. *J. Phys. Chem. Lett.* **2015**, *6*, 482−486.
(26) Shao, Y.; Xiao, Z.; Bi, C.; Yuan, Y.; Huang, J. Origin and Elimination of Photocurrent Hysteresis by Fullerene Passivation in $CH_3NH_3PbI_3$ Planar Heterojunction Solar Cells. *Nat. Commun.* **2014**, *5*, 5784.
(27) Stranks, D. S.; Snaith, J. H. Metal-halide perovskites for photovoltaic and light-emitting devices. *Nat. Nanotechnol.* **2015**, *10*, 391−402.
(28) Park, N. G. Organometal Perovskite Light Absorbers Toward a 20% Efficiency Low-Cost Solid-State Mesoscopic Solar Cell. *J. Phys. Chem. Lett.* **2013**, *4*, 2423−2429.
(29) Guerrero, A.; Juarez-Perez, J. E.; Bisquert, J.; Mora-Sero, I.; Garcia-Belmonte, G. Electrical field profile and doping in planar lead halide perovskite solar cells. *Appl. Phys. Lett.* **2014**, *105*, 133902.
(30) Liu, Y.; Sun, Y.; Rockett, A. A New Simulation Software of Solar Cells—wxAMPS. *Sol. Energy Mater. Sol. Cells* **2012**, *98*, 124−128.
(31) Yella, A.; Heiniger, L.-P.; Gao, P.; Nazeeruddin, M. K.; Grätzel, M. Nanocrystalline Rutile Electron Extraction Layer Enables Low-Temperature Solution Processed Perovskite Photovoltaics with 13.7% Efficiency. *Nano Lett.* **2014**, *14*, 2591−2596.
(32) Liu, F.; Zhu, J.; Wei, J.; Li, Y.; Lv, M.; Yang, S.; Zhang, B.; Yao, J.; Dai, S. Numerical Simulation: Toward the Design of High-Efficiency Planar Perovskite Solar Cells. *Appl. Phys. Lett.* **2014**, *104*, 253508.
(33) De Wolf, S.; Holovsky, J.; Moon, S.-J.; Löper, P.; Niesen, B.; Ledinsky, M.; Haug, F.-J.; Yum, J.-H.; Ballif, C. Organometallic Halide Perovskites: Sharp Optical Absorption Edge and its Relation to Photovoltaic Performance. *J. Phys. Chem. Lett.* **2014**, *5*, 1035−1039.
(34) Leijtens, T.; Lim, J.; Teuscher, J.; Park, T.; Snaith, H. J. Charge Density Dependent Mobility of Organic Hole-Transporters and Mesoporous TiO_2 Determined by Transient Mobility Spectroscopy: Implications to Dye-Sensitized and Organic Solar Cells. *Adv. Mater.* **2013**, *25*, 3227−3233.

DOI: 10.1021/acs.jpcc.5b06859
J. Phys. Chem. C 2015, 119, 22812−22819